

Adaptive observations using HSV and TESV in a 4D-Var framework with a finite volume shallow-water model

I. M. Navon*

Dept. of Mathematics and School of Computational Science
and Information Technology , Florida State University
Tallahassee, FL 32306, USA

Yanhua Cao

School of Computational Science
and Information Technology , Florida State University
Tallahassee, FL 32306, USA

Dacian N. Daescu

Department of Mathematics and Statistics,
Portland State University,
P.O. Box 751, Portland, OR 97207, USA

June 19, 2007

With 12 figures and 1 table

*Corresponding author: School of Computational Science and Information Technology, Florida State University, Tallahassee, FL 32306-4120

Abstract

A comparative analysis of observation targeting methods based on total energy singular vectors (TESVs) and Hessian singular vectors (HSVs) is performed with a finite volume global shallow-water model, along with its first and second order adjoint model. A 4D-Var data assimilation framework is considered that allows for adaptive observations distributed in both time and space domain. To obtain the HSVs a generalized eigenvalue problem was solved using the generalized Jacobi-Davidson algorithm. A full 4D-Var procedure without incremental approximation was used leading to an accurate second order adjoint and derivation of a consistent Hessian matrix. Numerical experiments involving TESV and HSV as alternative targeting strategies were carried out to assess the potential benefits of targeting methods using second order adjoint information.

The results obtained point to an advantage of using HSV as a tool for observation targeting where interaction between targeted observations taken at distinct instants in time has a significant impact on efficiency of both adaptive strategies. Additional metrics such as similarity indices between HSV and TESV also point to the same conclusion.

1 Introduction

Singular vectors identify directions in phase space which provide the maximum growth over a finite period in time with respect to specified norms.

Several techniques have been put forward to identify optimal sites for additional observations. Adjoint based techniques such as sensitivity to initial conditions and singular vectors (have been proposed) have been tested for such tasks by many groups of researchers.

As summarized by Langland (2006) targeted observing is a process in which supplementary atmospheric observations are assimilated to improve analyses in selected regions of the atmosphere, and reduce the uncertainty in forecasts of weather events that have large societal or economic impact.

Initial efforts were carried out by Lorenz and Emanuel (1998), Berliner et al. (1999), Barkmeijer et al. (1998), Leutbecher (2003), Langland et al. (1999), Pu and Kalnay (1999), Morss et al. (2001), Baker and Daley (2000). It has become evident through the work of Barkmeijer et al. (1998, 1999) that use of Hessian singular vectors (HSVs) where the Hessian of the cost function (if the background error and observation errors are uncorrelated) is equal to the inverse of the analysis error covariance matrix (Rabier and Courtier 1992, Fisher and Courtier 1995) holds promise for improving adaptive targeting observations. A methodology of interactive adaptive observations distributed in both time and space was introduced by Daescu and Carmichael (2003) and Daescu and Navon (2004) while the impact of data interaction on targeted observations with a 4-D Var data assimilation and forecast system was presented by Daescu et al. (2007). See also the relevant work of Bergot and Doerenbecher (2002), Bergot (2001), Buizza and Montani (1999), Palmer et al. (1998), Langland and Baker (2004) and Langland (2005).

The advantage of using HSVs (apart from the overhead to have to solve a generalized eigenvalue problem) is that initial time HSVs evolve into leading vectors of the propagated analysis error covariance at verification time.

Barkmeijer et al. (1998, 1999) have shown that the Hessian of the cost function in a variational data assimilation scheme can be used to compute SVs that incorporate an estimate of the full analysis error covariance at initial time. The resulting SVs, referred to as Hessian SVs or (HSVs), are consistent with the data assimilation scheme used to construct the forecast initial conditions. The HSVs also reflect the background and observational error correlations assumed by the data assimilation scheme (Gelaro et al. 2002).

The computational cost of obtaining the HSVs is several times greater than that of the TESVs, since they require solving a generalized eigenvalue problem (Davidson 1975), which precludes the use of the Lanczos algorithm. For a complete survey of second order methods in data assimilation see Le Dimet et al. (2002). In the present paper we present a comparison of TESVs and HSVs for observation targeting using a global shallow-water equations (SWE) model. See Lin and Rood (1997), Lin and Rood (1996), Lin et al. (1994) and Lin (2004) as well as Akella and Navon (2006).

The paper plan is the following.

In section 2 a brief description of the fvSW global model is provided along with the first and second order adjoint required for the HSV research. The generalized Jacobi-Davidson algorithm and its application in the frame work of the JDQZ package as developed by Sleijpen et al. (1996) and Bai, Sleijpen and Van der Vorst (1999) is briefly described in section 3. In section 4 we review the application of TESV and HSV methods for targeting observations and describe the scenarios of interaction of fixed and adaptive observations. Detailed numerical results are presented in section 5 looking at the differences between HSVs and TESVs in a framework of adaptive observations targeting. Discussion of results of similarity index between TESVs and HSVs is presented in section 6. Conclusions and summary along with further research directions are presented in Section 7.

2 Brief description of Lin Rood fvSW along with its first and second order adjoint models

The numerical model used in this paper is a finite volume two-dimensional global shallow-water (SW) model. The SW equations in spherical coordinates in the vorticity divergence form assume the following form

$$\frac{\partial h}{\partial t} + \nabla \cdot (\mathbf{V}h) = 0 \quad (1)$$

$$\frac{\partial u}{\partial t} = \Omega v - \frac{1}{a \cos \theta} \frac{\partial}{\partial \lambda} [\kappa + \varphi] \quad (2)$$

$$\frac{\partial v}{\partial t} = -\Omega u - \frac{1}{a} \frac{\partial}{\partial \theta} [\kappa + \varphi] \quad (3)$$

where h represents the fluid height (above the surface height, h_s), $\mathbf{V} = (u, v)$ represent the zonal and meridional wind velocity components respectively. The free surface geopotential height is given by $\varphi = \varphi_s + gh = gh_s + gh$, $\kappa = \frac{1}{2} \mathbf{V} \cdot \mathbf{V}$ is the kinetic energy, and $\Omega = 2\omega \sin \theta + \nabla \times \mathbf{V}$ is the absolute vorticity, ω is the angular velocity of the earth.

The finite volume shallow water equations model of Lin and Rood (1997) has been used for integrating the above SW equations. The advection schemes have been implemented in two dimensions by using a sequential operator-split approach, details of which have been provided in Lin and Rood (1996). A two grid combination based on C-grid and D-grids has been used while advancing from time step t_n to t_{n+1} . In the first half of the time step, the advective winds (time centered winds on the C-grid: $(u^*; v^*)$) are updated the C-grid, and in the other half of the time step, the prognostic variables $(h; u; v)$ are updated on the D-grid (in this study, we will use the same advection scheme on both the grids).

The explicit finite-volume flux-form semi-Lagrangian (FFSL) scheme of Lin and Rood (1997) at a $5^\circ \times 5^\circ$ resolution and a constant time step $\Delta t = 900s$ are used. As a reference initial state x_0^{ref} the 500mb ECMWF ERA-40 data valid for March 15, 2002 06h

is considered. The model state at the initial time and after 24h integration is displayed in Fig. 1.

4-D Var data assimilation experiments are setup in a twin experiments framework. A background field x_b is prescribed using a shift method in the reference initial state. The background state at the initial time and after 24h integration is displayed in Fig. 2. The 24h forecast error $x_v^{ref} - x_v^b = M(x_0^{ref} - x(x_b))$ in a total energy metric exhibits a large magnitude over the domain $D_v = [120^\circ W, 100^\circ W] \times [34^\circ N, 51^\circ N]$ that is defined as the verification domain at $t_v=24h$ (which is defined to be the verification time). Here x_v^{ref} is the verifying analysis at t_v .

In Fig. 3, we show the errors between the background field and the reference state at the initial time and the 24h forecast, respectively, evaluated in the total energy norm

$$\langle \delta x(\lambda, \theta), \delta x(\lambda, \theta) \rangle = \frac{1}{2}[(\delta u)^2 + (\delta v)^2] + \frac{1}{\phi_0}(\delta \phi)^2, \quad (4)$$

where

$\delta x(\lambda, \theta) = x(\lambda, \theta) - x^{ref}(\lambda, \theta)$, ϕ_0 is the mean geopotential height of the reference data at the initial time.

The adjoint method application in variational data assimilation provides a way of obtaining the exact gradient of the cost function (which uses the prognostic variables of the model) with respect to the model initial conditions. The first order adjoint model satisfies two properties. It is the transpose of the tangent linear model (TLM) and also it allows for obtaining the exact gradient of the cost function with respect to the control variables. In this paper 4-D Var data assimilation is performed in the assimilation window $[0, 6]$ h and it is assumed that routine observations are only available at $t=6h$ on a coarse $10^\circ \times 10^\circ$ grid. The error in the forecast initiated from the analysis obtained is also shown in Fig. 4. From this figure it can be seen that after data assimilation the error over the entire domain is reduced, however it still remains the largest error over the verification domain. Hence adaptive observations are necessary.

Other than the first order adjoint method additional information may be obtained by using the second order adjoint method. Here a second order adjoint model (SOA) was used which has been developed for the above mentioned global S-W equations model. One integration of the SOA model yields a value of the Hessian (the matrix of second partial derivatives) multiplied by a vector or a column of the Hessian of the cost function with respect to the initial conditions. The SOA model yields the Hessian of the cost function which is related to the inverse of the analysis error covariance matrix that may be approximated by the inverse Hessian matrix of the cost functional in the 4-D Var, i.e to solve

$$(\mathbf{PM})^* \mathbf{E} (\mathbf{PM}) v = \sigma^2 \mathbf{A}^{-1} v \quad (5)$$

in the optimization interval $t_v - t_i$.

The specification of the metrics \mathbf{E} and \mathbf{A}^{-1} at time t_v and t_i , respectively, is discussed by Palmer et al. (1998). Here \mathbf{P} is a diagonal projection operator on verification domain D_v satisfying $\mathbf{P}^* \mathbf{P} = \mathbf{P}^2 = \mathbf{P}$. The generalized eigenvalue problem above can be solved using the JDQZ package (See Sleijpen et al. 1996, Fokkema et al. 1998).

The proposed Jacobi-Davidson method (Sleijpen and Van der Vorst 1996) can solve the generalized eigenvalue problem without using explicit knowledge of the operators on both sides of the equation. We make use of this algorithm to determine Hessian singular vectors using the 4-D Var variational assimilation Hessian as a constraint at initial time.

3 Description of HSV and TESV and the generalized eigenvalue problem

Consider the 2-D global shallow-water equations model, its tangent linear model can be written as $\delta x_t = \mathbf{M}(t, 0) \delta x_0$, where δx_t is the evolution of perturbation at time t , δx_0 is the initial perturbation at initial time 0, and $\mathbf{M}(t, 0)$ is a linearized version of the original non-linear operator. In the present case we consider perturbations of the state vector δx which consists of $(\delta\phi; \delta u; \delta v)$ at initial time.

In order to compute the fastest growing perturbations at a target time, it is necessary to define an inner product of the linear vector space of perturbations. We define the inner product $(x, y) = \langle x, \mathbf{E}y \rangle$, where $\langle \cdot ; \cdot \rangle$ denotes a Euclidean inner product and \mathbf{E} denotes the total energy norm. For $x = (\phi; u; v)$, it yields the form

$$\|x\|_{\mathbf{E}}^2 = (x, x) = \langle x, \mathbf{E}x \rangle = \int_{\Sigma} \left[\frac{1}{2}u^2 + \frac{1}{2}v^2 + \frac{\phi^2}{\phi_0} \right] d\Sigma \quad (6)$$

It is obvious that \mathbf{E} is a positive-definite diagonal matrix.

Singular vectors depend on norms that are used to measure their amplitude at initial and final time.

Singular vectors optimized for total energy at verification time in the verification region are employed to identify sensitive regions of the atmosphere, where initial-condition error is likely to contribute most to the forecast error.

In this paper we consider SVs, which maximize the ratio at optimization time t

$$\frac{\|x_t\|_{\mathbf{E}}^2}{\|x_0\|_{\mathbf{A}^{-1}}^2} = \frac{\langle x_t, \mathbf{E}x_t \rangle}{\langle x_0, \mathbf{A}^{-1}x_0 \rangle} = \frac{\langle \mathbf{M}x, \mathbf{E}\mathbf{M}x_0 \rangle}{\langle x_0, \mathbf{A}^{-1}x_0 \rangle} = \frac{\langle x_0, \mathbf{M}^*\mathbf{E}\mathbf{M}x_0 \rangle}{\langle x_0, \mathbf{A}^{-1}x_0 \rangle} = \lambda^2 \quad (7)$$

where the superscript " * " represents the transpose.

This suggests solving the generalized eigenvalue problem

$$\mathbf{M}^*\mathbf{E}\mathbf{M}v_i = \lambda_i^2 \mathbf{A}^{-1}v_i \quad (8)$$

The generalized eigenvectors v_i and the generalized eigenvalues λ_i are respectively called the SVs and singular values of \mathbf{M} (with respect to \mathbf{A}^{-1} norm). They are orthogonal and form a complete basis. Any x_i can therefore be expressed as a linear combination of the SVs v_i . The leading SVs are sometimes called optimal perturbations and the time during which perturbation grows is considered the optimization time.

In practice, one can only compute a small number of SVs compared with the huge dimension of the model variables. In order to make the SVs more relevant to limited target area domain, Barkmeijer (1992) introduced a local projection operator \mathbf{P} , which

sets model variables to zero outside the concerned domain. Then the ratio is generalized as

$$\lambda^2 = \frac{\langle \mathbf{P}x_t, \mathbf{E}\mathbf{P}x_t \rangle}{\langle x_0, \mathbf{A}^{-1}x_0 \rangle} \quad (9)$$

The eigenvalue problem becomes

$$(\mathbf{P}\mathbf{M})^*\mathbf{E}(\mathbf{P}\mathbf{M})v_i = \lambda_i^2 \mathbf{A}^{-1}v_i \quad (10)$$

In the computation of the TESVs, the total energy metric is used at initial and optimization time, i.e. \mathbf{E} and \mathbf{A}^{-1} are identical. In the case of HSVs, the inverse of the analysis error covariance matrix is used to define the norm at initial time. The operator \mathbf{A}^{-1} is specified to be equal to the full Hessian of the 4-D Var cost function. It has turned out that of the simple metrics considered, the total energy metric is the most consistent with the analysis-error statistics. In Barkmeijer et al. (1998) a method is proposed to make the singular vector computation fully consistent with the analysis error statistics by employing the Hessian of the 3-D Var cost function.

The HSVs are calculated with an initial-time norm based on the Hessian of the 4-D Var cost function which provides an estimate of the analysis error covariance. For observation targeting, the norm defined with the inverse of the analysis error covariance is the adequate choice as structures with equal amplitude represent equally likely initial errors, given the fact that the analysis error is normally distributed (Barkmeijer et al. 1998; Palmer et al. 1998).

Both types of singular vectors are normalized to have unit total energy at initial time. The weight given to the contribution from singular vector j is its singular value σ_j in order to emphasize the structures that are likely to contribute most to the forecast error. The function F ranks geographical locations (λ, θ) according to the sensitivity of the forecast to errors of the initial condition at that location. The target region is defined as the set

$$D = \{(\lambda, \theta) | F(\lambda, \theta) > F_c\}, \quad (11)$$

in which F exceeds a threshold value F_c . The value of F_c is adjusted in order to obtain a target region with a pre-specified area (details see Daescu and Navon, 2003).

It was found by Leutbecher et al. (2002) that the HSV targeting is superior to the TESV targeting results.

4 Computational aspects of the Hessian singular vectors

Barkmeijer et al. (1998) introduced Hessian singular vectors and showed how they could be derived from the iterative solution of a generalized eigenvalue problem.

In computation of singular vectors one has to specify a norm at initial time t_0 and at optimization time t , where singular vectors v are considered maximizing the ratio (9), where (\cdot, \cdot) is the Euclidean inner product. \mathbf{A}^{-1} and \mathbf{E} are symmetric positive definite operators and \mathbf{P} is a projection operator setting a vector to zero outside a given domain.

The singular vectors are solutions of the generalized eigenvalue problem (10). The adjoint operators \mathbf{M}^* and \mathbf{P}^* are determined with respect to the Euclidean inner product.

In calculation of HSV the operator \mathbf{A}^{-1} is equal to the Hessian of the 4-D Var cost function with respect to the control variables while \mathbf{A}^{-1} is not known in matrix form and determining its square root is not feasible. Barkmeijer et al. (1999) have shown that one can solve (10) by a generalized Davidson algorithm. This algorithm can solve (10) efficiently and requires only the capability of solving $y = Sx$ where S is any of the operators $\mathbf{M}, \mathbf{P}, \mathbf{E}$ or \mathbf{A}^{-1} . No explicit knowledge of any operator is needed. We will briefly outline the algorithm of the package JDQZ used for solving the generalized eigenvalue problem (10) in appendix A. (See Fokkema et al. 1998, Sleijpen and Van der Vorst 1996, Sleijpen et al. 1996, also Leutbecher 2003).

5 Numerical experiments

In this section adaptive targeting strategies using the leading total energy singular vectors (TESVs) and the leading Hessian singular vectors (HSVs) are analyzed for the global finite volume shallow water equations model and the experimental settings are described in above section 2. We assume that at each time step in the assimilation window $[0,6]$ h five adaptive observations are selected using a singular vector targeting strategy. A comparative performance analysis is presented for different experiments: In the first experiment we assume that only routine observations are available to the data assimilation process. In the second and third experiments we assume that both routine observations as well as adaptive observations are available for the TESV and HSV targeting methods, respectively. However the routine observations are only available on a $10^\circ \times 10^\circ$ coarser mesh. For each experiment and for each of the targeting methods the data assimilation procedure is performed using the M1QN3 large-scale limited-memory unconstrained minimization routine, which based on a limited-memory quasi-Newton method. (see Liu and Nocedal 1989, Gilbert and Lemarechal 1989). For each targeting method, the minimization process of the cost functional J (over the entire domain) provides the analysis initial condition x_0^a . The evolution of the normalized forecast error reduction $J_v(x_0^a)/J_v(x_0)$ at the verification time over the verification domain is also monitored. The total energy norm is used to define the inner product $\langle \cdot, \cdot \rangle_{\mathbf{E}}$ and to quantify the forecast error formula at verification time.

To implement the TESV and HSV method, 10 leading singular values and their associated singular vectors were computed at each targeting instant using the ARPACK package (Lehoucq et al. 1998) and the JDQZ package implementing the Davidson generalized eigenvalue solver (Sleijpen et al. 1996 and Sleijpen, Van der Vorst and Bai 1999) respectively. The evolution of the first total energy singular vector and Hessian singular vector for the 500mb geopotential height field for an optimization interval $[t,24]$ h with $t=2\text{h},4\text{h},6\text{h}$ are shown in Fig. 5.

Similarly, the time evolution of the first total energy singular vector and Hessian singular vector of the zonal wind field and of the meridional wind field are shown in Figs. 6 and 7, respectively.

We begin our analysis by presenting the results obtained for TESV and HSV methods. The evolution of the sensitivity field corresponding to the Hessian singular vectors method and the total energy singular vectors method are shown in Fig. 8. Adaptive observations using total energy singular method are marked with ' Δ ' while adaptive locations marked with ' σ ' in Fig. 8 were selected from the Hessian singular vector method.

For each targeting method, the distribution of the forecast error at the verification time over the verification domain after data assimilation takes place is shown in the total energy norm in Fig. 9. The forecast error using the background estimate as the initial conditions is also displayed in Fig. 9 as a reference.

The potential forecast improvement using adaptive observations is limited by various factors such as the accuracy and formulation of the background estimate, the configuration of the existing observational network, the length of the verification time, and the number of additional observational resources allocated, etc. As it can be seen in Fig. 11 the HSV method provides the best forecast over D_v at t_v , but there is only little improvement as compared to the TESV method outside of D_v . Even in some other domain the error is bigger than TESV method. One should notice that by using adaptive observations we only attempt to improve the forecast over a given sub-domain at a given future time.

6 Similarity Index between TESVs and HSVs

In adaptive observations information about analysis errors impacts on both observing locations and the optimal sampling strategy (Baker and Daley 2000).

Using HSVs which are consistent with the data assimilation used to construct the forecast initial conditions in a full 4-D Var setup should enhance results of adaptive observations targeting.

To assess the differences between the subspaces spanned by the leading TESVs and HSVs we use a projection matrix to exhibit the difference between TESVs and HSVs (Buizza 1994). The projection matrix is defined as,

$$m_{i,j}(TESV, HSV) = [\langle v_i(TESV), \mathbf{E}v_j(HSV) \rangle]^2 \quad (12)$$

Each element of above projection matrix is the squared scalar product of the i th TESV and the j th HSV. It represents the amount of energy of the j th HSV that is explained by the i th TESV. The sum of the matrix elements with a fixed index represents how well the j th HSV can be reconstructed from a linear combination of the first i th TESV.

In Table 1 if the projection matrix element is less than 1 then it is set to be 0. The projection matrix (Table 1) shows that at initial time the seventh HSV resembled by the eighth TESV, the seventh HSV resembled by the ninth TESV, these two SVs are the 'meteorological' ones in the sense of Buizza et al. (1993) for HSV. At time ($t_i=6$ h) the fourth HSV resembled by the sixth TESV, this SVs is the 'meteorological' ones.

Also we can use another measure of similarity based on projection of a set of singular vectors on another is provided by the similarity index of the TESV and HSV (Buizza 1994), that is,

$$s(TESV, HSV; N) = \frac{1}{N} \sum_{i,j=1}^N m_{i,j}(TESV, HSV) \quad (13)$$

(which measures the similarity between the unstable subspaces spanned by the first N SVs of TESV and HSV). The index goes from 1 for parallel unstable subspaces to 0 when the subspaces are orthogonal.

Figure 12 shows the similarity index (based on the total energy norm) of the 10 leading TESVs and HSVs at initial time for different forecast hour. Results are presented for the leading 3, 5, 7, 9, and 10 SVs for every hour of the study period.

Also we carried out experiments about the leading 10 SVs for the initial time and final time (24 hours forecast) as in Gelaro et al (2002). The average similarity index between

the TESV and HSV unstable subspaces is about 0.03 when the subspaces were spanned by the leading ten singular vectors at initial time. However after evolving for 24 hours, the similarity index increased to 0.19. These outputs are very similar to the results obtained by Gelaro.

7 Summary and conclusions

In this study leading TESVs and HSVs singular vectors techniques have been employed to identify optimal sites for taking additional observations. These methods are tested in the context of 4-D Var data assimilation using a finite volume global shallow-water equations model. We first carried out a comparison between TESVs and HSVs. The method described in this paper uses the full Hessian (or second derivative) of the cost function of the variational data assimilation with respect to the initial conditions as control parameters to obtain the leading HSVs. These are related to the inverse analysis error covariance matrix (Fisher 2001). In this way the calculation of singular vectors can be made consistent with the 4-D Var calculation of the analyzed state. To obtain the HSVs a generalized eigenvalue problem was solved using the Jacobi-Davidson algorithm (Davidson 1975) methodology. The algorithm is implemented the JDQZ package developed by Sleijpen et al. (1996) and Sleijpen, Van der Vorst and Bai (1999).

As shown in Daescu and Navon (2004), in order to fully account for the temporal dimension of the 4-D Var scheme, multiple targeting instants must be considered in the assimilation window. The present work represents a first step in the design of optimal sampling strategies for time distributed adaptive observations in the framework of 4-D Var. In particular, it is shown that the combined results of TESV and HSV targeted observations taken at distinct instants in time yield a significant impact on the efficiency of the adaptive targeting strategies.

Results of our analysis carried out in the 4-D Var framework for a global 2D shallow-water model shows that Hessian singular vectors may serve to provide an improved model

forecast as compared to using only the leading total energy singular vectors.

Our future research will focus on the extending of present targeting methods using Hessian singular vectors for operational atmospheric models. A rigorous theoretical framework to account for time distributed adaptive observations remains to be formulated.

Further studies will also be related to the impact of the structure of the background error covariance on the outcome of above experiments.

Acknowledgments

The first 2 authors would like to acknowledge support of NSF grant ATM 0201808 managed by Dr J. Fein. They would like also to thank Professor Gerard L.G. Sleijpen Mathematical Institute, Utrecht University, and the Netherlands for making available to us the code JDQZ for solution of generalized eigenvalue problems. The second and third authors also acknowledge support from NASA Modeling, Analysis and Prediction Program under award NNG06GC67G.

References

- Akella S, Navon IM (2006) A comparative study of the performance of high resolution advection schemes in the context of data assimilation. *International Journal for Numerical Methods in Fluids*, **51 (7)**, 719-748
- Bai Z, Demmel J, Dongarra J, Ruhe A and van der Vorst H (2000) editors, Templates for the solution of Algebraic Eigenvalue Problems: A Practical Guide. *SIAM, Philadelphia*, 440pp
- Bai Z., Sleijpen G and van der Vorst H (2000) Quadratic Eigenvalue Problems (Section 9.2). in Z. Bai, J. J. Demmel, J. J. Dongarra, A. Ruhe, and H. A. van der Vorst, Templates for the Solution of Algebraic Eigenvalue Problems - A Practical Guide, pages 281-289, SIAM, Philadelphia, Pa., 2000.
- Baker NL, Daley R (2000) Observation and background adjoint sensitivity in the adaptive observation-targeting problem. *Q.J.R. Meteorol. Soc.*, **126**, 1431-1454
- Barkmeijer J, Buizza R, Palmer TN (1999) 3D-Var Hessian singular vectors and their potential use in the ECMWF Ensemble Prediction System. *Q.J.R. Meteorol. Soc.*, **125**, 2333-2351
- Barkmeijer J, Van Gijzen M, Bouttier F (1998) Singular vectors and estimates of the analysis-error covariance metric. *Q.J.R. Meteorol. Soc.*, **124**, 1695-1713
- Barkmeijer J (1992) Local error growth in a barotropic model. *Tellus* , **44A (4)**, 314-323
- Beck A, Ehrendorfer M (2005) Singular-vector-based covariance propagation in a quasi-geostrophic assimilation system. *Mon. Wea. Rev.*, **133 (5)**, 1295-1310
- Bergot T, Hello G, Joly A, and Malardel S (1999) Adaptive observations: A feasibility study. *Mon. Wea. Rev.*, **127 (5)**, 743-765
- Bergot, T., and A. Doerenbecher, 2002: A study on the optimization of the deployment of targeted observations using adjoint-based methods. *Q.J.R. Meteorol. Soc.*, 128, 1689-1712.
- Bergot T (2001) Influence of the assimilation scheme on the efficiency of adaptive obser-

- vations. *Q.J.R. Meteorol. Soc.*, **127**, 635-660.
- Berliner LM, Lu Z-Q, Snyder C (1999) Statistical design for adaptive weather observations. *J. Atmos. Sci.*, **56**, 2536-2552
- Bishop CH, Toth Z (1999) Ensemble transformation and adaptive observations. *J. Atmos. Sci.*, **56**, 1748-1765
- Bishop CH, Etherton BJ, Majumdar SJ (2001) Adaptive sampling with the ensemble transform Kalman filter. Part I: Theoretical aspects. *Mon. Wea. Rev.* **129**, 420-436
- Buizza R, Tribbia J, Molteni F, Palmer T (1993) Computation of optimal unstable structures for a numerical weather prediction model. *Tellus*, **45A**, 388-407
- Buizza R (1994) Localization of optimal perturbations using a projection operator. *Q. J. R. Meteorol. Soc.*, **120**, 1647C1681
- Buizza R, Montani A (1999) Targeted observations using singular vectors. *J. Atmos. Sci.* **56**, 2965-2985
- Cardinali C, Buizza R (2003) Forecast skill of targeted observations: A singular-vector-based diagnostic. *J Atmos Sci*, **60 (16)**, 1927-1940
- Daescu DN, Carmichael GR (2003) An adjoint sensitivity method for the adaptive location of the observations in air quality modeling. *J. Atmos. Sci.*, Vol. **60**, No. 2, 434-450
- Daescu D.N. and Navon IM (2004) Adaptive observations in the context of 4D-Var data assimilation. *Meteorol. Atmos. Phys.*, **85**, 205-226
- Daescu DN, Navon IM, Akella S, Erlebacher G (2007) The Impact of Data Interaction on Targeted Observations with a 4D-Var Data Assimilation System. *The 11th Conference on Integrated Observing and Assimilation Systems for Atmosphere, Oceans, and Land Surface (IOAS-AOLS), 87th AMS Annual Meeting, San Antonio, TX 14-18 January 2007*
- Daescu, DN and Navon IM (2007) Efficiency of a Pod-based reduced second order adjoint model in 4-D VAR data assimilation. *International Journal for Numerical Methods in Fluids*, **53**, 985-1004

- Davidson ER (1975) Iterative calculation of a few of lowest eigenvalues and corresponding eigenvectors of large real-symmetric matrices. *Journal of Computational Physics*, **17** (1), 87-94.
- Doerenbecher A, Bergot T (2001) Sensitivity to observations applied to FASTEX cases. *Nonlinear Processes in Geophys.*, **8**, 467-481
- Doerenbecher A, Fourrié N, Leutbecher M, Majumdar S, Petersen GN (2005) Insight into the meaning of North Atlantic TReC 2003 Hessian singular vectors based sensitive areas. *Geophysical Research Abstracts*, **7**, 08632.
- Fisher M. and Courtier P. (1995) Estimating the covariance matrices of analysis and forecast errors in variational data assimilation. **ECMWF Tech Memorandum**, **220**, 28pp.
- Fokkema DR, Sleijpen GLG, and van der Vorst HA (1998) Jacobi-Davidson style QR and QZ algorithms for the reduction of matrix pencils *SIAM J. Sc. Comput.*, **20:1**, 94-125pp.
- Fokkema DR and van Gijzen MB (1999) Short manual for the JDQZ-package. 8pp. Available from www.math.uu.nl/people/sleijpen/JDsoftware/manual.ps.gz.
- Gelaro R, Rosmond T, and Daley R (2002) Singular Vector Calculations with an Analysis Error Variance Metric. *Mon. Wea. Rev.*, **130**, 1166-1186
- Kim HM, Morgan MC, and Morss RE (2004) Evolution of Analysis Error and Adjoint-Based Sensitivities: Implications for Adaptive Observations. *J Atmos Sci*, **61**, 795-812
- Kucukkaraca E. and Fisher M (2006) Use of analysis ensembles in estimating flow-dependent background error variances. *ECMWF Technical Memorandum*, 492. *European Centre for Medium-Range Weather Forecasts (ECMWF), Reading, UK.*
- Jacobi C (1846) Ueber ein leichtes Verfahren, die in der Theorie der Sacularstorungen vorkommenden Gleichungen numerisch aufzulösen. *J. Reine Angew. Math.*, 51-94pp.
- Langland RH, Gelaro R, Rohaly GD, Shapiro MA (1999) Targeted observations in FASTEX: Adjoint-based targeting procedures and data impact experiments in IOP17 and

- IOP18. *Q.J.R. Meteorol. Soc.*, **125**, 3241-3270
- Langland RH (2005) Issues in targeted observing. *Q.J.R. Meteorol. Soc.*, **131**, 3409-3425
- Langland RH, and Baker NL (2004) Estimation of observation impact using the NRL atmospheric variational data assimilation adjoint system. *Tellus*, **56A**, 189-203
- Le Dimet FX, Navon IM, and Daescu DN (2002) Second Order Information in Data Assimilation. *Mon. Wea. Rev.*, **130 (3)**, 629-648
- Leutbecher M, Barkmeijer J, Palmer TN, and Thorpe AJ (2002) Potential improvement to forecasts of two severe storms using targeted Observations. *Q. J. R. Meteorol. Soc.*, **128**, 1641-1670pp.
- Leutbecher M (2003) A reduced rank estimate of forecast error variance changes due to intermittent modifications of the observing network. *J. Atmos. Sci.*, **60**, 729-742
- Lin S-J, Chao WC, Sud YC, Walker GK (1994) A class of the van Leer transport schemes and its applications to the moisture transport in a general circulation model. *Mon. Wea. Rev.*, **122**, 1575 -1593
- Lin S-J (2004) A vertically Lagrangian finite-volume dynamical core for global models. *Mon Wea Rev*, **132**, 2293 -2307
- Lin S-J, and Rood RB (1996) Multidimensional flux-form semi-Lagrangian transport schemes. *Mon Wea Rev*, **124**, 2046 -2070
- Lin S-J, and Rood RB (1997) An explicit flux-form semi-Lagrangian shallow-water model on the sphere. *Q.J.R. Meteorol. Soc.*, **123**, 2477-2498
- Lorenz EN, Emanuel KA (1998) Optimal sites for supplementary weather observations: Simulation with a small model. *J. Atmos. Sci.*, **55**, 399-414
- Majumdar SJ, Aberson SD, Bishop, CH, Buizza R, Peng MS, and Reynolds CA (2006) A comparison of adaptive observing guidance for Atlantic tropical cyclones. *Mon. Wea. Rev.*, **134**, 2354-2372
- Moler CB, and Stewart GW (1973) An algorithm for generalized matrix eigenvalue problems. *SIAM J. Numer. Anal.*, **10**, 241-256

- Morss RE, Emanuel KA, Snyder C (2001) Idealized adaptive observation strategies for improving numerical weather prediction. *J. Atmos. Sci.*, **58** 210-234
- Palmer TN, Gelaro R, Barkmeijer J, and Buizza R (1998) Singular vectors, metrics, and adaptive observations. *J. Atmos. Sci.*, **55**, 633-653
- Pu Z-X, and Kalnay E (1999) Targeting observations with the quasi-inverse linear and adjoint NCEP global models: Performance during FASTEX. *Quart. J. Roy. Meteor. Soc.*, *125*, 3329-3337
- , –, Sela J, and Szunyogh I (1997) Sensitivity of forecast errors of initial conditions with a quasi-inverse linear method. *Mon. Wea. Rev.*, **125**, 2479-2503
- Rabier F, Courtier P (1992) 4-Dimensional assimilation in the presence of baroclinic instability. *Quart J R Meteorol Soc*, **118 (506)**, 649-672 Part A.
- Sleijpen GLG, Booten AGL, Fokkema, DR, et al. (1996) Jacobi-Davidson type methods for generalized eigenproblems and polynomial eigenproblems. *BIT*, **36 (3)**, 595-633
- Sleijpen GLG, Vander Vorst HA (1996) A Jacobi-Davidson iteration method for linear eigenvalue problems. *SIAM Journal on Matrix Analysis and Applications*, **17 (2)**, 401-425
- Szunyogh I, Toth Z, Morss RE, Majumdar SJ, Etherton BJ, Bishop CH (2000) The effect of targeted dropsonde observations during the 1999 winter storm reconnaissance program. *Mon. Wea Rev.* **128**, 3520-3537
- Szunyogh I, Toth Z, Majumdar SJ, Morss R, Bishop C, and Lord S, (1999) Ensemble-based targeted observations during NORPEX. *Preprints, Third Symp. on Integrated Observing Systems, Dallas, TX, Amer. Meteor. Soc.*, 74-78
- , –, Morss RE, Majumdar SJ, Etherton BJ, and Bishop CH (2000) The effect of targeted dropsonde observations during the 1999 Winter Storm Reconnaissance Program. *Mon. Wea. Rev.*, **128**, 3520-3537
- , –, Zimin AV, Majumdar SJ, and Persson A (2002) Propagation of the effect of targeted observations: The 2000 Winter Storm Reconnaissance Program. *Mon. Wea.*

Appendix A A Brief summary of Jacobi-Davidson algorithm as implemented in JDQZ.

The Jacobi-Davidson method constructs accurate approximations (μ, λ, x) of the generalized eigenvalue problem

$$\mu Ax = \lambda Bx \tag{A-1}$$

where A and B are $(n \times n)$ matrices, x is a non-trivial n -vector. μ, λ belong to a 1-D complex, projective plane. We scale μ to 1 and $\lambda \in C$. The idea of Jacobi-Davidson method (see Sleijpen and Van der Vorst 1996) is to construct a correction for a given eigenvector approximation in a subspace orthogonal to the given approximation.

The small projected problem is then reduced to a generalized Schur form by the QZ method of Moler and Stewart (1973). The JDQZ method used for solving the generalized eigenvalue problem produces a partial generalized Schur form of the generalized eigenproblem.

By using implicit restarts techniques and preconditioning one finally obtains the resulting algorithm JDQZ (see Fokkema et al. (1998), Sleijpen et al. (1996), Fokkema and Van Gijzen (1999) JDQZ manual).

This algorithm is available in FORTRAN and is also enhanced with a deflation technique allowing several solutions of the eigenproblem to be computed.

For practical applications see the manual of Fokkema and Van Gijzen (1999) describing in some detail the FORTRAN code of JDQZ which is calling the libraries of LAPACK and BLAS.

The user should supply three problem dependent routines, namely a vector matrix multiplier with operator A called AMUL, one for multiplication with B called BMUL and a routine for performing the preconditioning operation which must be called PRECON.

The preconditioning will speed the convergence of JDQZ, but is not impacting on the final result.

In the present paper the Hessian singular vector calculation is controlled using the JDQZ package. The calculation will stop when the maximum number of iterations has been performed, or when the maximum number singular vectors have been calculated. JDQZ calculates the Hessian singular vectors as the solutions to the following generalized eigenvector equation

$$\mathbf{M}^*\mathbf{P}^*\mathbf{E}\mathbf{P}\mathbf{M}x = \lambda\mathbf{J}''x \quad (\text{A-2})$$

where \mathbf{M} denotes the tangent linear model, \mathbf{M}^* is the transpose of \mathbf{M} , \mathbf{E} defines the inner product at optimization time, \mathbf{P} is a projection operator over a verification domain, outside the domain the value will be set to 0, and \mathbf{J}'' is the Hessian of 4-D Var cost function which is the inner product at initial time. The algorithm requires operators which apply $\mathbf{M}^*\mathbf{P}^*\mathbf{E}\mathbf{P}\mathbf{M}$ and \mathbf{J}'' to arbitrary vectors. These operations are represented in the code by the subroutines AMUL and BUML respectively. Subroutine BMUL calculates a Hessian-vector product as a second order adjoint model for the input vector.

JDQZ starts with an initial matrix \mathbf{V} . The columns of \mathbf{V} are orthonormalized with respect to the initial time inner product. That is, they are made to satisfy $\mathbf{V}^*\mathbf{J}''\mathbf{V} = \mathbf{I}$.

Next, the following small ordinary eigenvalue problem is solved

$$\mathbf{V}^*\mathbf{M}^*\mathbf{P}^*\mathbf{E}\mathbf{P}\mathbf{M}\mathbf{V}y = \theta y \quad (\text{A-3})$$

The eigenvalues of this problem are the Ritz values (i.e. approximations to the eigenvalues) of (refeigen). The residual, $r = \mathbf{M}^*\mathbf{P}^*\mathbf{E}\mathbf{P}\mathbf{M}\mathbf{V}y - \theta\mathbf{J}''\mathbf{V}y$ for the leading unconverged Ritz value is selected. The residual is orthogonal to the columns of \mathbf{M} in the Euclidean sense.

A vector which is orthogonal with respect to the Hessian is produced by first calculating an approximate solution to the linear equation $\mathbf{J}''v = r$, and then explicitly orthonormalizing v . The accuracy of the solution is determined by TOL (the required

reduction in the norm of the error), and MAXSTEP (the maximum number of iterations to be performed).

Once the vector v has been determined, it is included as a new column of \mathbf{V} , and the process is repeated. It can be shown that if the linear equation $\mathbf{J}''v = r$ is solved exactly, then the algorithm is equivalent to a Lanczos algorithm. If it is solved approximately, the algorithm resembles the Jacobi-Davidson method.

Figure Captions

Figure 1. The configuration of the model state for the reference run (x_0^{ref}): 500mb geopotential height and velocities field at the initial time and after a 24h forecast.

Figure 2. The configuration of the background state (x_b): 500mb geopotential height and velocities field at the initial time and after a 24h forecast.

Figure 3. Distribution of the forecast error in total energy norm at the initial time and $t=24$ h using the reference state and the background estimate as the initial condition respectively. The verification domain $\mathcal{D}_v = [120^\circ\text{W } 100^\circ\text{W}] \times [34^\circ\text{N } 51^\circ\text{N}]$ is shown with solid line.

Figure 4. Distribution of the forecast error in total energy norm at $t=24$ h using the analysis state in data assimilation which is performed with observations from fixed locations only ($10^\circ \times 10^\circ$ coarse grid) as the initial condition. The verification domain $\mathcal{D}_v = [120^\circ\text{W } 100^\circ\text{W}] \times [34^\circ\text{N } 51^\circ\text{N}]$ is shown with solid line.

Figure 5. Time evolution of the first total energy singular vector and Hessian singular vector in 500mb geopotential height field for the optimization interval $[t_i, 24]$ h respectively. Results shown for $t_i = 2\text{h}, 4\text{h}, 6\text{h}$.

Figure 6. Time evolution of the first total energy singular vector and Hessian singular vector in zonal wind field for the optimization interval $[t_i, 24]$ h respectively. Results shown for $t_i = 2\text{h}, 4\text{h}, 6\text{h}$.

Figure 7. Time evolution of the first total energy singular vector and Hessian singular vector in zonal wind field for the optimization interval $[t_i, 24]$ h respectively. Results shown for $t_i = 2\text{h}, 4\text{h}, 6\text{h}$.

Figure 8. Time evolution of the sensitivity field and adaptive observation locations using the leading Hessian singular vectors method (marked with 'o') (HSV) and using the leading total energy singular vectors method (marked with ' Δ ') (TESV). Results shown for $t_i = 2\text{h}, 4\text{h}, 6\text{h}$.

Figure 9. Distribution of the forecast error at the verification time over the verification domain when data assimilation is performed using both routine and adaptive observations provided by the different targeting methods, respectively. For reference, the results between the reference state and the background state and the results obtained by using routine observations only are also displayed.

Figure 10. Top: The minimization of the cost function J when both routine and adaptive observations provided by different targeting methods respectively, are assimilated. Middle: During the minimization process the evolution of the gradient. Normalized values are shown on a logarithmic scale. Bottom: During the iterative process, for each targeting method the forecast error reduction at the verification time over \mathbf{D}_v is quantified by evaluating the ratio $J_v(x_0^a)/J_v(x_0)$. For reference, the results obtained using routine observations only are also displayed.

Figure 11. Distribution of the forecast error in total energy norm at the verification time when data assimilation is performed with routine and adaptive observations pro-

vided by different targeting methods, respectively. Significant forecast improvement may be observed over the verification domain. However outside the verification domain little forecast improvement can be observed.

Figure 12. Subspace similarity for the leading 3, 5, 7, 9, 10 TESVs and HSVs at different forecast time. See text for details.

Table 1. The projection matrix for TESV and HSV. The indices on the first row refer to HSV and the indices on the first column to TESV. Each entry $m_{i,j}$ of the matrix gives the square scalar product between the i th TESV and the j th HSV. That is, the percentage of energy of the j th HSV explained by the i th TESV. The last row gives the percentage of energy of the j th HSV by all leading 10 TESVs. Top: projection matrix at $t_i=0$ h Bottom: projection matrix at $t_i=6$ h.

Unstable sub-space projection matrix for TESVs and HSVs at $t_i=0h$

	1	2	3	4	5	6	7	8	9	10
1	3	0	3	0	2	1	8	0	2	0
2	6	0	0	0	0	3	0	0	0	0
3	2	2	0	0	2	0	1	0	4	2
4	0	0	4	1	0	0	1	0	1	1
5	4	0	2	4	9	8	5	0	5	0
6	0	0	0	0	0	0	8	0	0	0
7	1	0	0	0	0	4	5	1	3	0
8	1	0	0	2	1	5	11	0	1	1
9	1	0	0	2	2	1	10	0	0	5
10	0	0	1	0	0	0	0	0	7	8
total	22	4	13	12	18	25	53	4	26	15

Unstable sub-space projection matrix for TESVs and HSVs at $t_i=6h$

	1	2	3	4	5	6	7	8	9	10
1	0	1	0	0	0	0	0	0	0	0
2	0	0	1	0	0	0	0	0	0	0
3	0	3	1	4	4	5	1	0	1	0
4	0	4	0	0	1	0	0	0	0	0
5	0	0	0	0	0	0	0	0	1	0
6	3	8	0	20	0	2	2	2	0	0
7	3	1	4	3	2	5	0	1	0	3
8	1	2	0	2	0	0	1	0	0	0
9	0	2	0	0	0	1	0	0	0	1
10	0	1	0	0	0	0	2	0	0	0
total	9	25	10	31	11	15	8	5	3	7

Table 1.

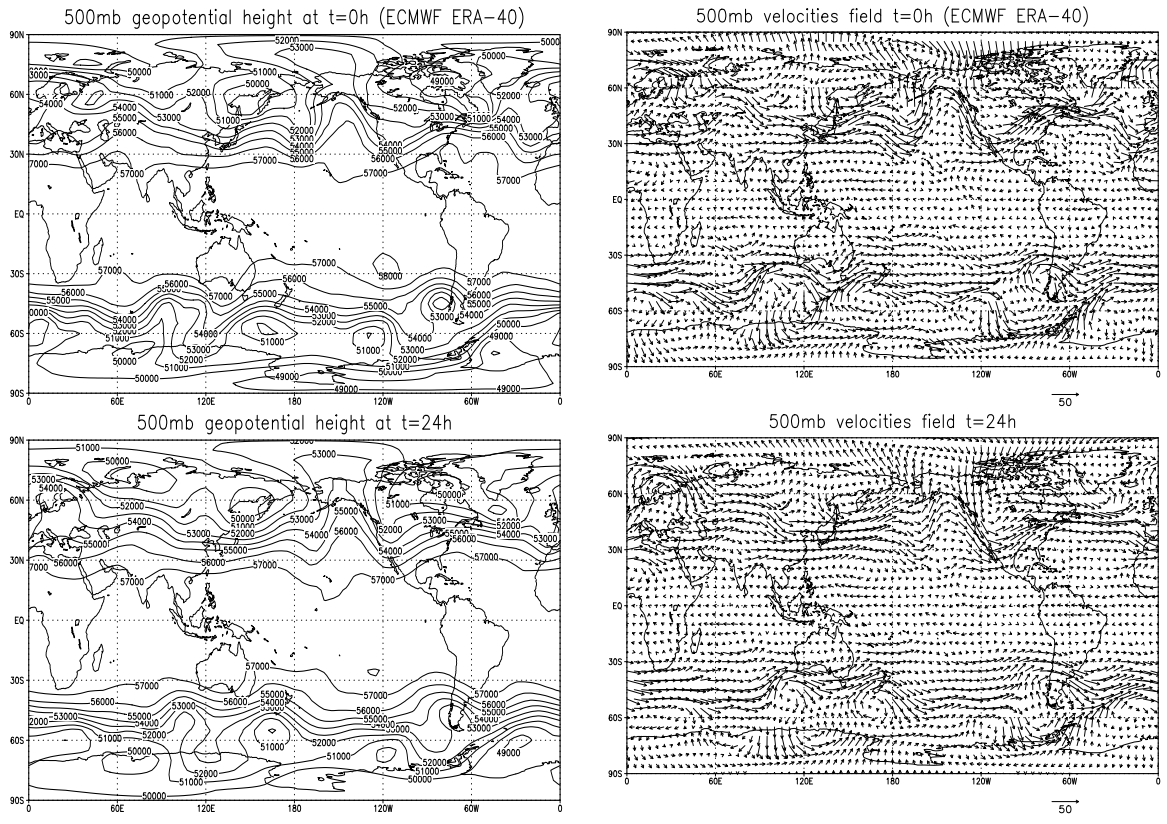


Figure 1:

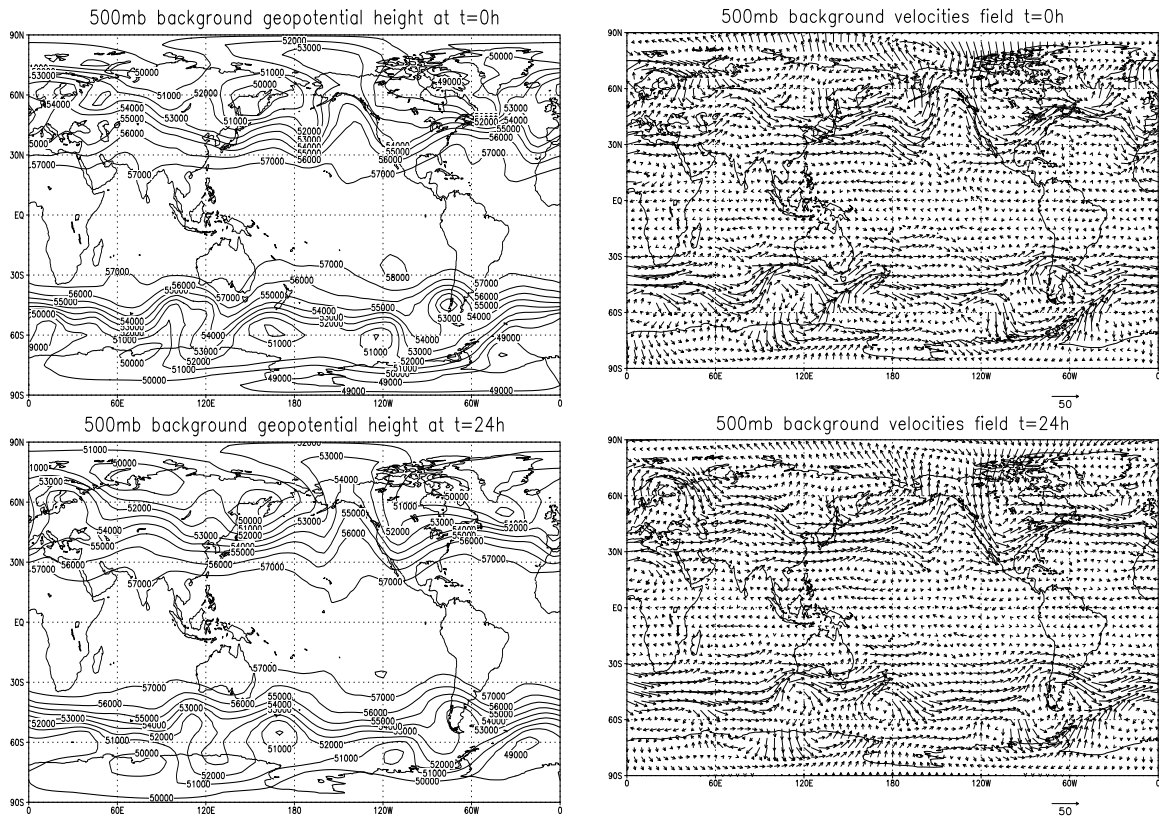


Figure 2:

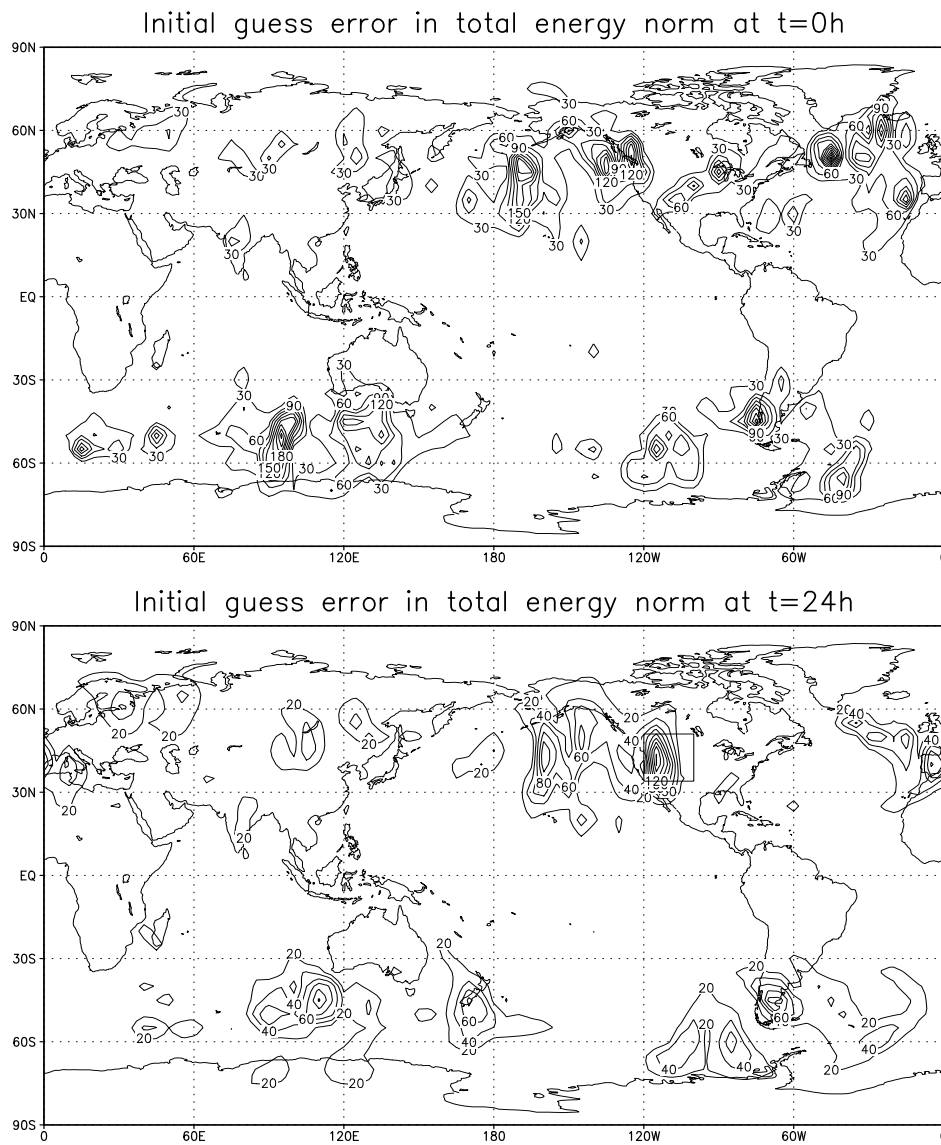


Figure 3:

Error (total energy norm) of 24h forecast with fixed obs only

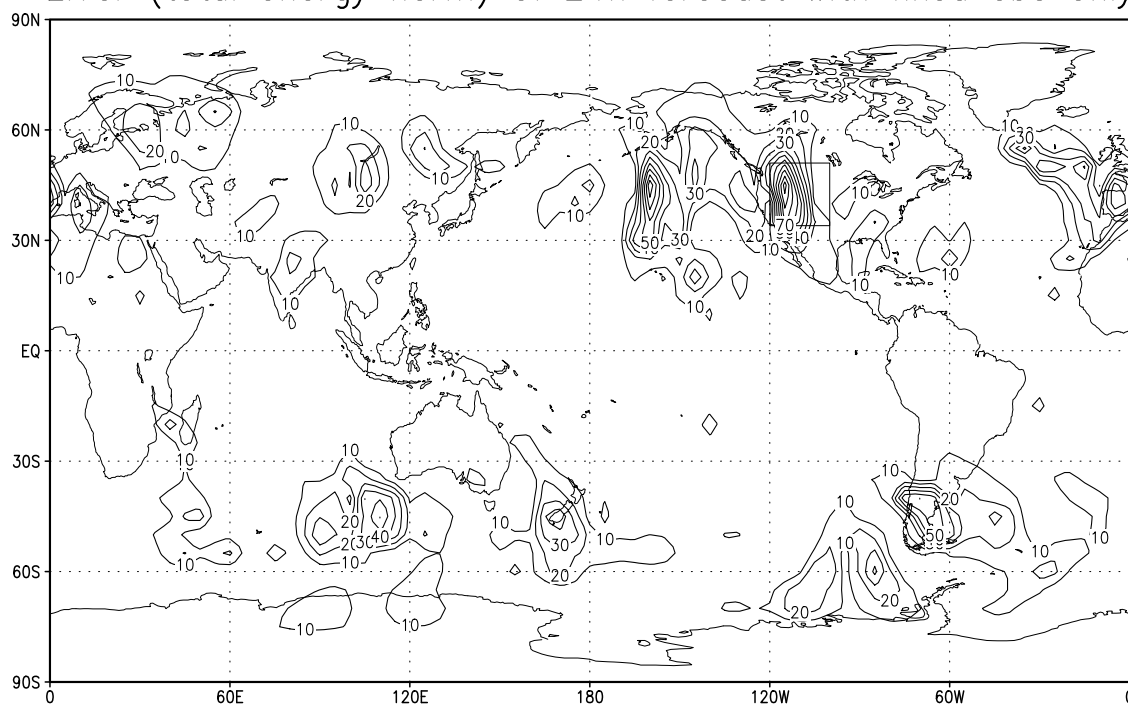


Figure 4:

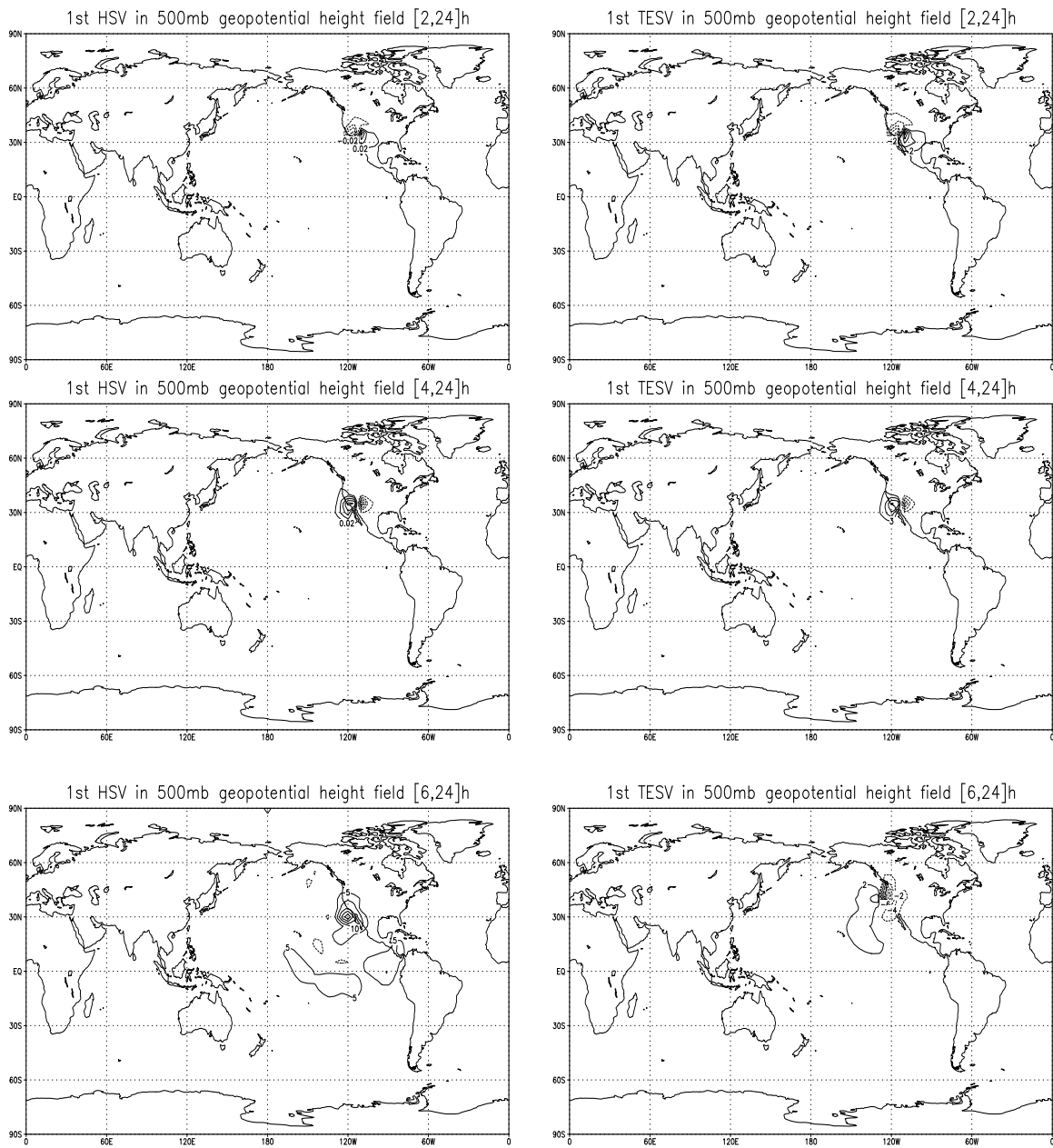


Figure 5:

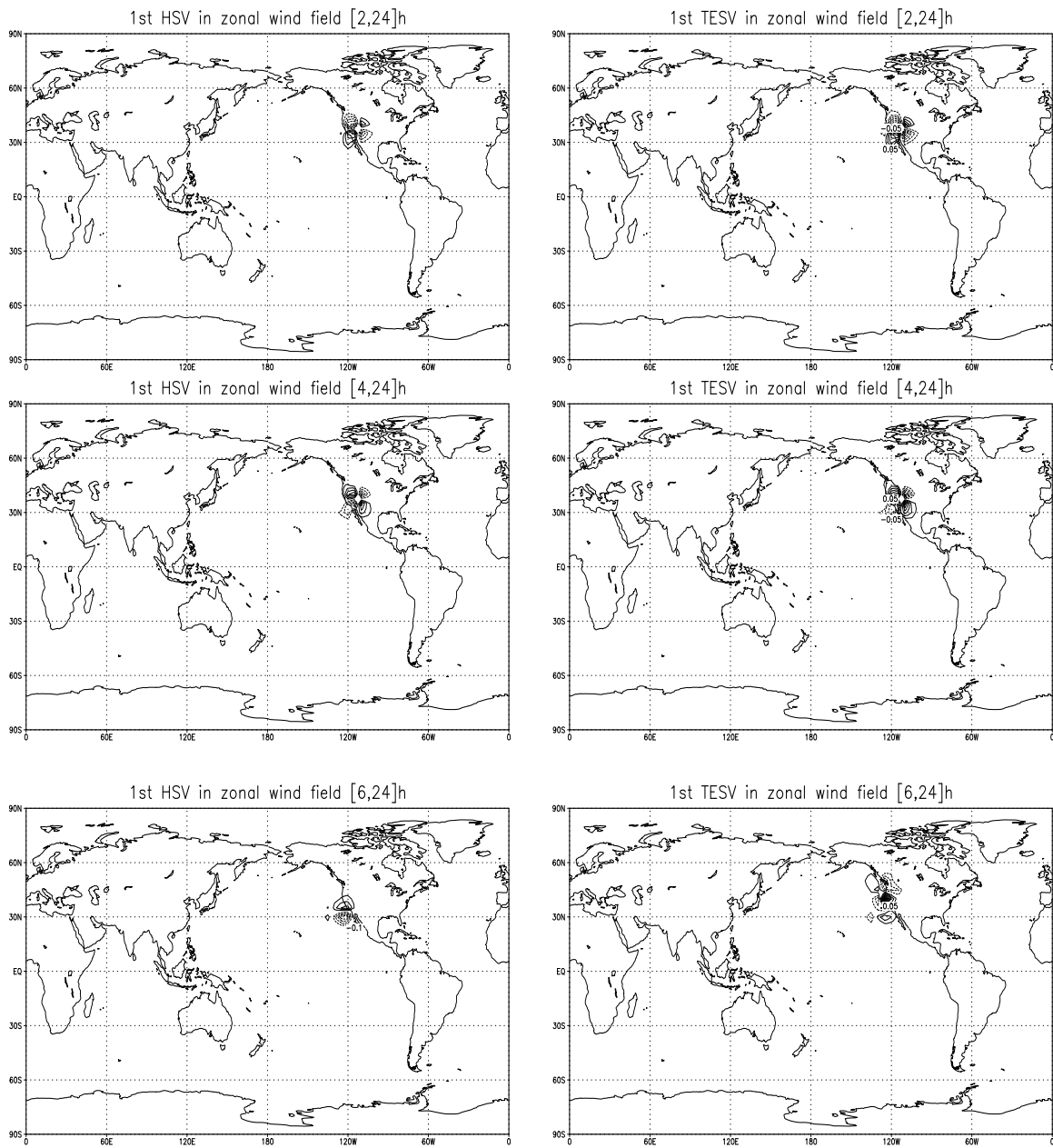


Figure 6:

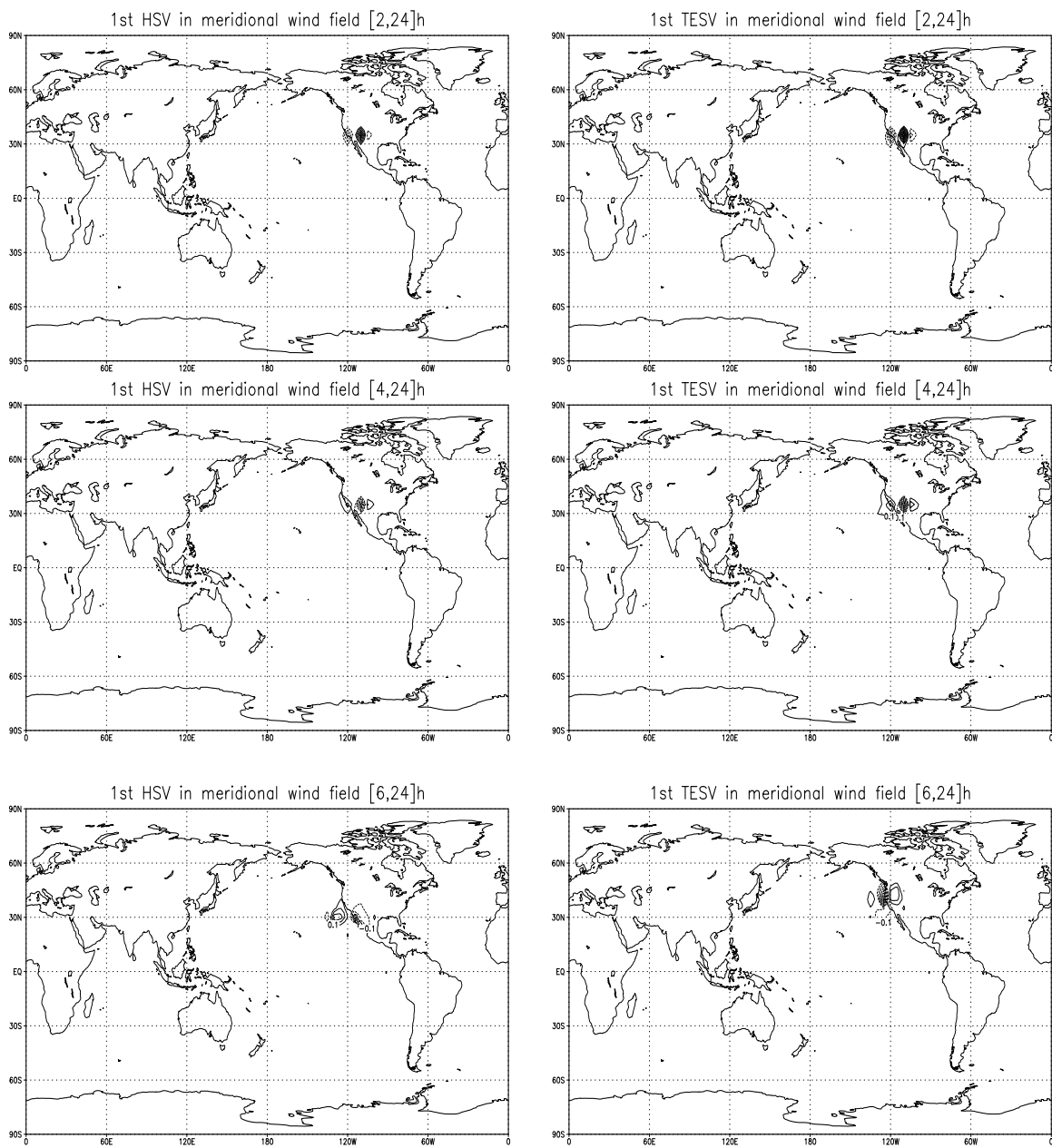


Figure 7:

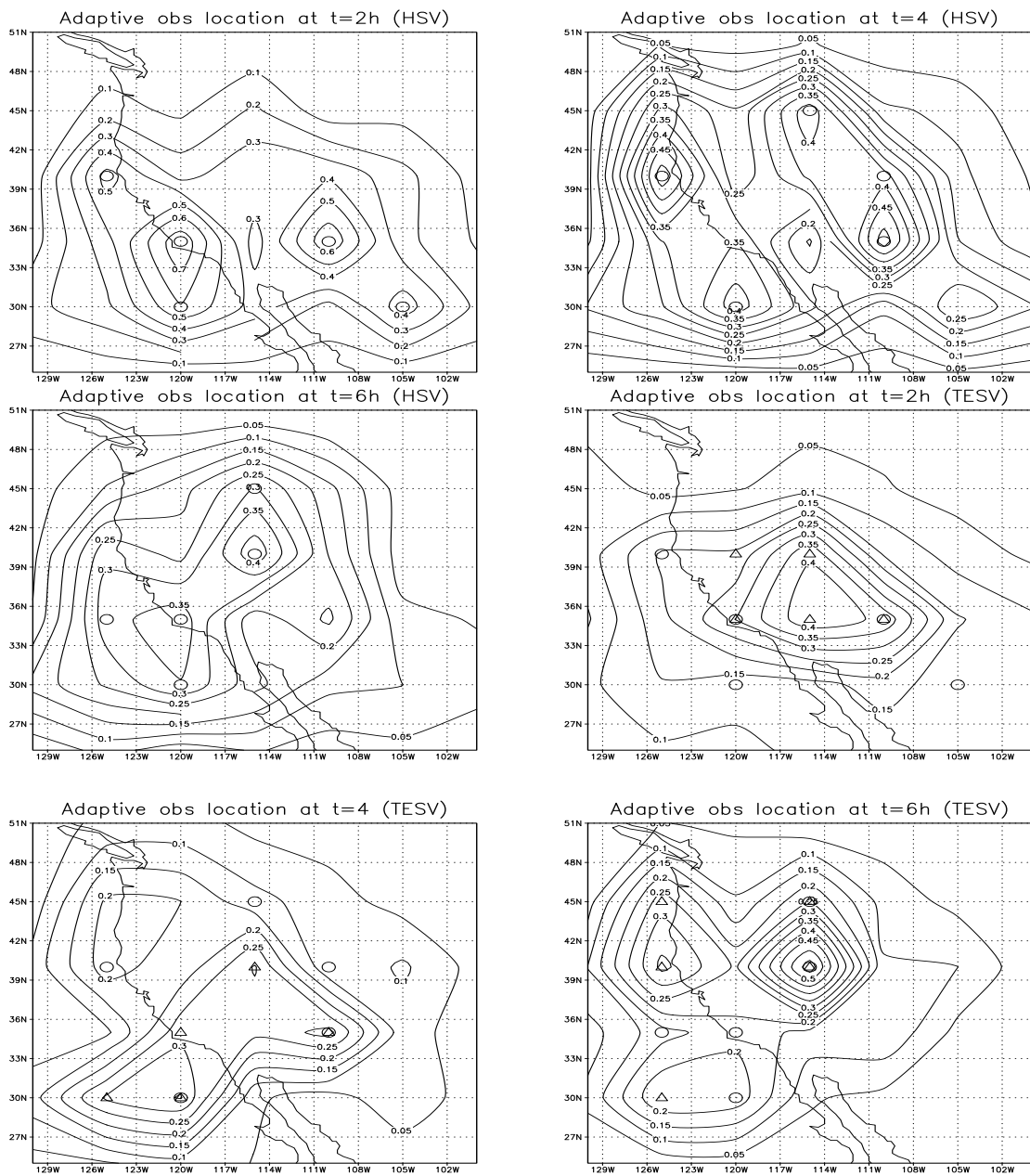
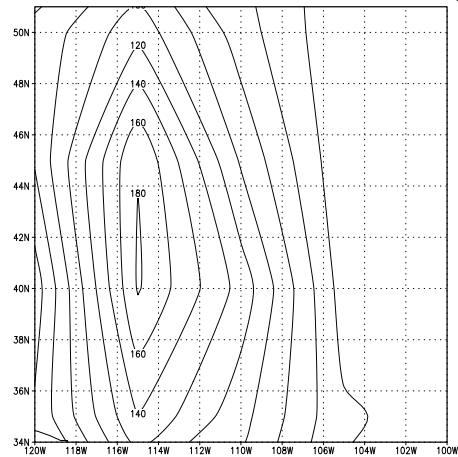
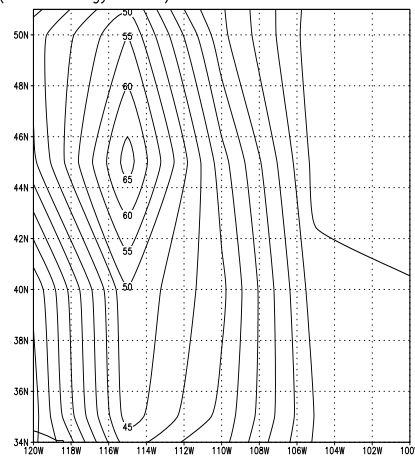


Figure 8:

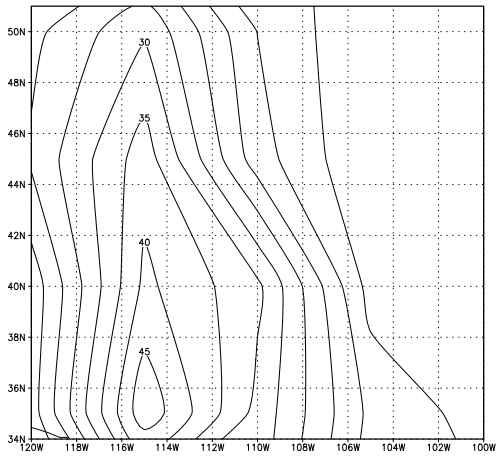
Error at 24h between the reference and the background



Error (total energy norm) of 24h forecast with fixed obs only



Error at 24h with fixed and adaptive obs (TESV)



Error at 24h with fixed and adaptive obs (HSV)

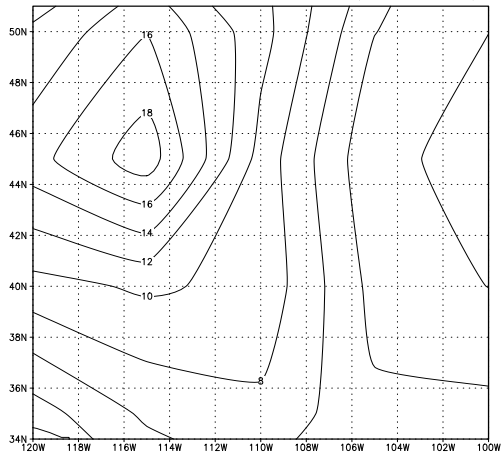


Figure 9:

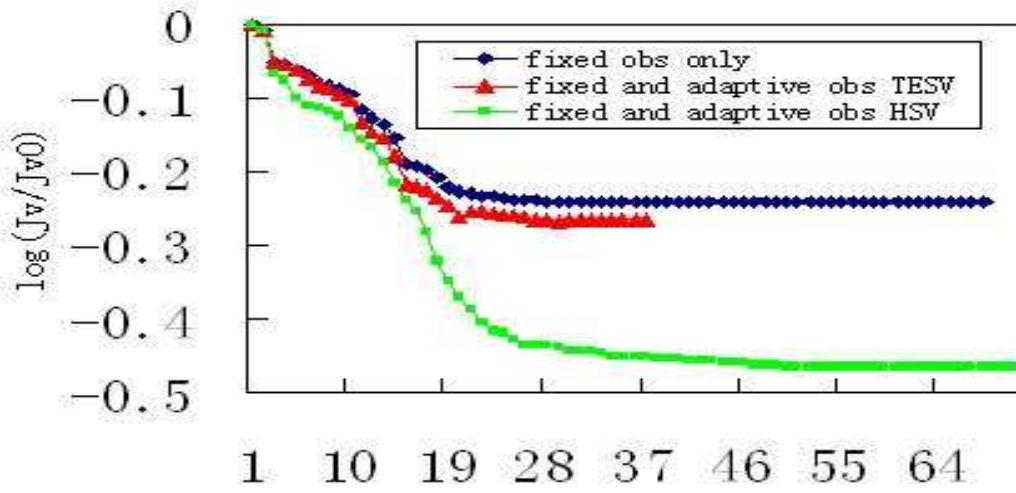
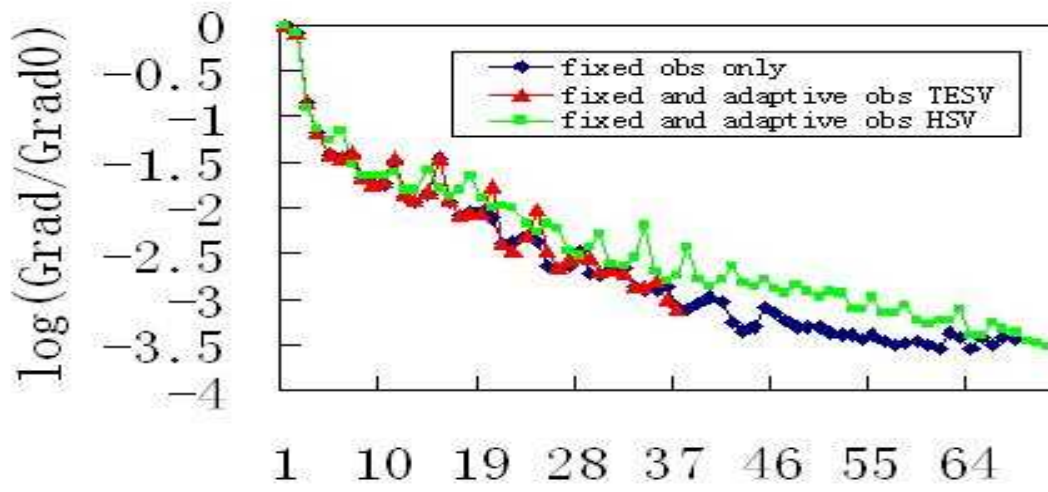
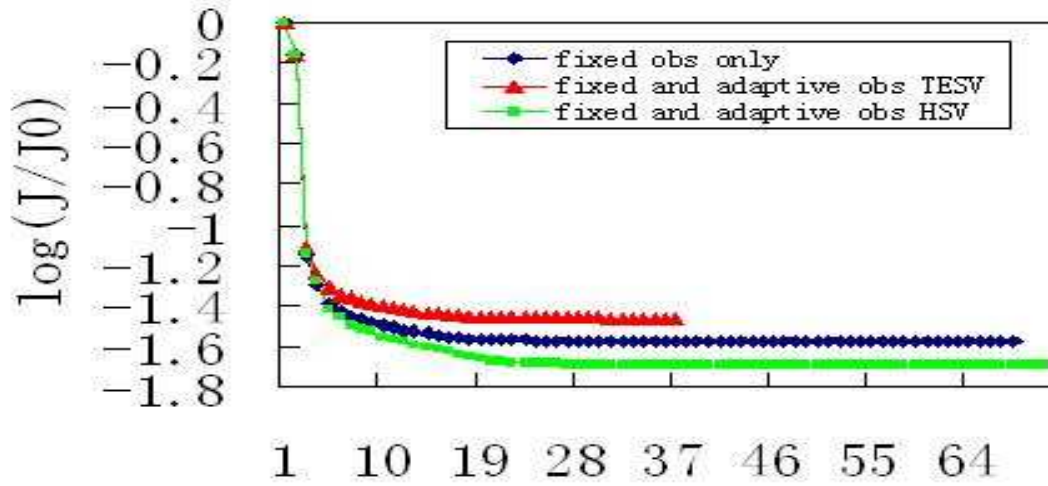


Figure 10:
36

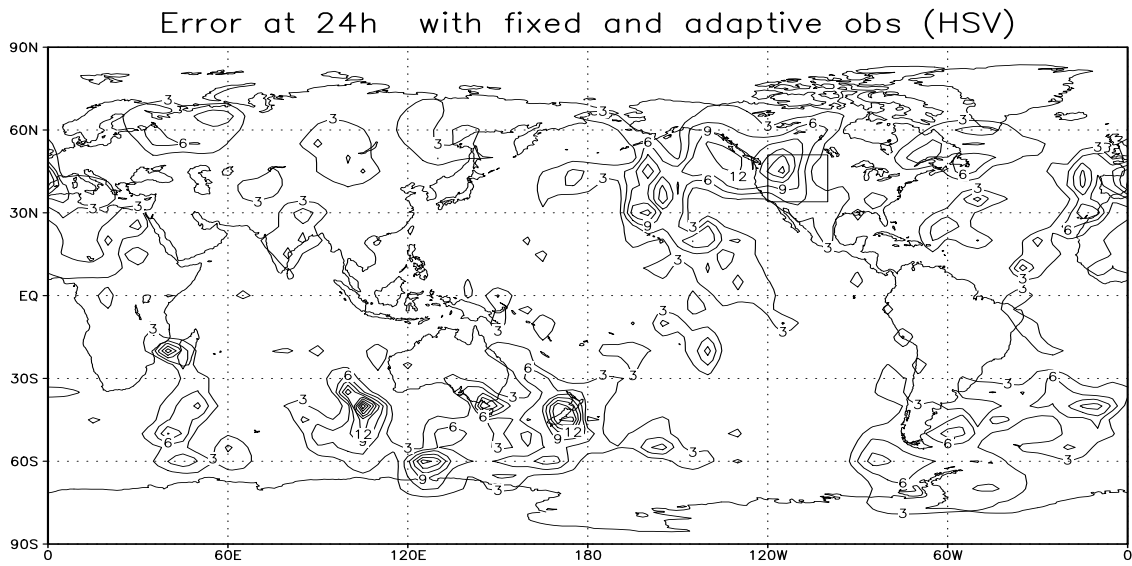
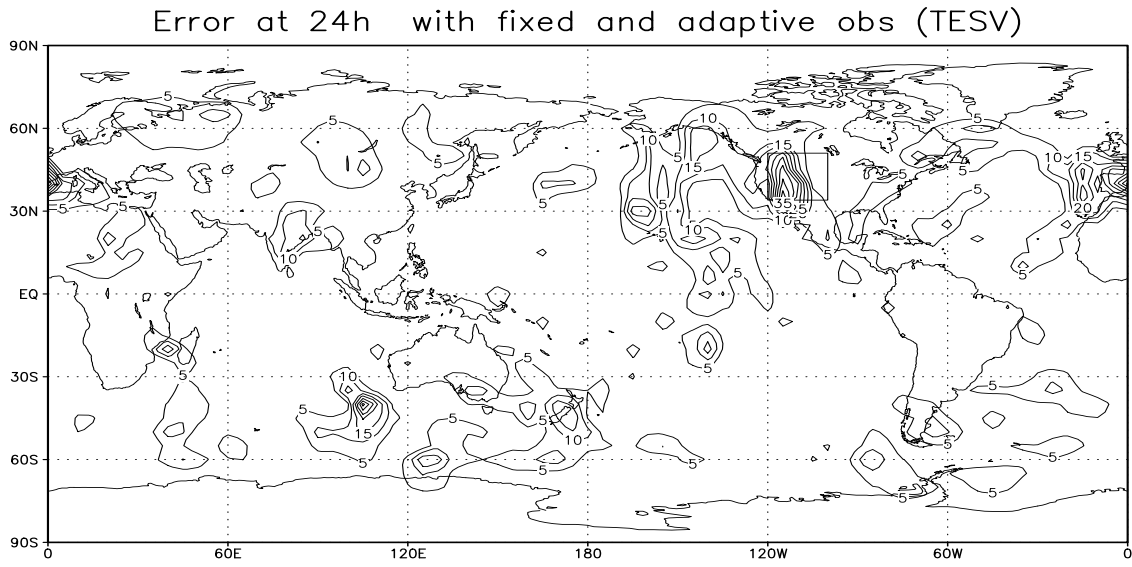


Figure 11:

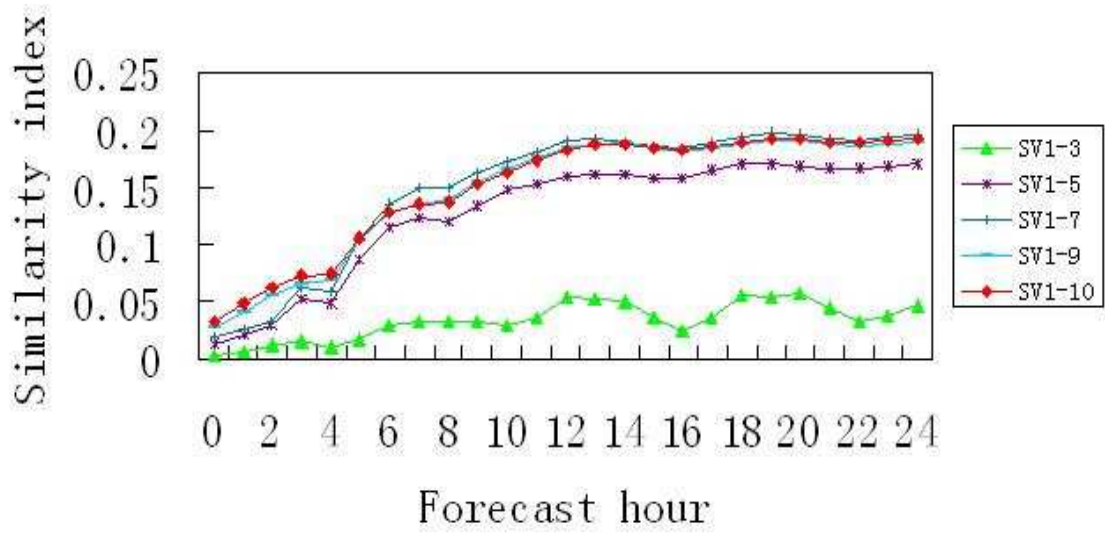


Figure 12: